Investigating Transmission Pathways of a Nosocomially Transmitted Fungal Infection

by

Md Mehadi Hasan

A thesis submitted to the Faculty of Graduate Studies of
The University of Manitoba
in partial fulfillment of the requirements of the degree of

Master of Science

Department of Mathematics
University of Manitoba
Winnipeg

Dedicated to my parents, my wife, and my supervisor for their unwavering support and encouragement.

Acknowledgements

First and foremost, I would like to express my deepest gratitude to Almighty Allah for granting me the strength, knowledge, ability, and opportunity to undertake this research and complete it successfully. Without His blessings, this achievement would not have been possible.

I am sincerely thankful to my supervisor, Dr. Julien Arino, Professor, Department of Mathematics, University of Manitoba, Canada. His guidance, insightful feedback, and open-door support were invaluable whenever I encountered challenges or had questions regarding my research or writing. He consistently encouraged me to pursue my ideas while providing direction when it was most needed.

Finally, I wish to express my heartfelt thanks to my parents and wife for their unwavering support and continuous encouragement throughout my academic journey and the process of completing this thesis. Their love, patience, and belief in me made this accomplishment possible.

Author

Md Mehadi Hasan

Post-Defence Acknowledgement

I would like to extend my sincere appreciation to the Defence Chair, Dr. Kang-Ling Liao, for moderating my thesis defence and ensuring the process was conducted smoothly and professionally. I am also deeply grateful to the Examining Committee - Dr. Julien Arino (Advisor), Dr. Stephanie Portet (Internal), and Dr. Christopher Heggerud (Internal) - for carefully reviewing my thesis, providing constructive feedback, and engaging in thoughtful discussion during the defence. Their valuable insights and suggestions have greatly improved the quality of this work.

Abstract

This thesis investigates the transmission dynamics of nosocomial fungal infections such as *Candida auris*, a multidrug-resistant pathogen increasingly observed in intensive care units (ICUs)-using both deterministic and stochastic (continuous-time Markov chain, CTMC) modelling approaches. Our compartmental framework includes patients, healthcare workers (HCWs), and the ICU environment, capturing multiple transmission pathways between these vectors. We examine outbreak dynamics through extinction analysis, basic reproduction number, sensitivity testing, and two-dimensional parameter interaction heatmaps. Our results show that environmental contamination and undetected infectious patients are primary drivers of transmission, with patient-origin outbreaks showing low extinction probabilities.

Contents

List of Figures

List of Tables

1

Introduction

Fungal infections (or mycoses) affect humans in various forms, ranging from mild skin conditions to invasive, life-threatening illnesses [7]. While viruses and bacteria have traditionally garnered more attention in medical research, there has been an increasing focus on fungal infections and their associated diseases in recent years. Understanding the characteristics, transmission dynamics, and management of fungal infections is essential for effective healthcare practices and patient safety.

One emerging nosocomial fungal pathogen that has attracted significant attention is *Candida auris* (*C. auris*). This multidrug-resistant yeast presents a serious global health threat because of its ability to cause severe infections with associated high mortality rates [15, 30]. *C. auris* has been reported in various countries worldwide. Its association with healthcare facilities, such as hospitals and long-term care facilities, is particularly concerning, as it can easily spread between patients and persist on surfaces and healthcare equipment, contributing to the potential for outbreaks within these settings [19, 27]. The impact of *C. auris* infections on patient safety cannot be overstated: mortality rates as high as 30% to 60% have been reported, surpassing those of other common fungal infections [15, 19].

Recent years have seen a growing interest in mathematical modelling of noso-

comial fungal pathogens, including *C. auris* to look at how it spreads in healthcare settings. These studies have investigated key factors, such as environmental contamination, transmission through healthcare workers, and patient susceptibility [10, 16, 17]. However, these factors are often examined separately, and few models have integrated all three within a single framework. This makes it harder to understand how they might interact in places like ICUs.

Such nosocomial fungal infections represent a critical concern, particularly for patients in intensive care units (ICUs), where vulnerable individuals are at high risk of developing such infections. Understanding the transmission dynamics in such settings of nosocomial fungal infections is essential. To this end, we develop a mathematical model to investigate key factors that may contribute to the spread of nosocomial fungal infections within ICUs. In our model, ICU patients are categorized into two distinct groups: uncolonized patients, who are susceptible to infection, and colonized patients, who have already contracted the disease. The isolated nature of ICU wards reduces direct patient-to-patient transmission, leading us to consider two primary routes for transmission from colonized to uncolonized patients: transmission facilitated by healthcare workers (HCWs) and transmission through the environment.

This thesis is organized as follows: we introduce an ODE model and its corresponding continuous-time Markov chain in Chapter 3, then in Chapter 4, conduct a mathematical analysis of the model. Chapter 5 presents a computational analysis of the model. A Discussion concludes the thesis.

2

Preliminaries

2.1 Ordinary differential equations

An ordinary differential equation (ODE) is an equation that relates a function to its derivatives. In general, an ODE describes how a vector-valued function $\boldsymbol{x}(t) \in \mathbb{R}^n$ evolves over time according to a specified rule. A system of first-order ODEs takes the form:

$$\frac{d\boldsymbol{x}_i}{dt} = \boldsymbol{F}_i(t, x_1, x_2, \ldots, x_n), \quad \boldsymbol{x}_i(t_0) = \boldsymbol{x}_i^0, \quad i = 1, \ldots, n, \tag{2.1.1}$$

where $\boldsymbol{F}_i : \mathbb{R}^{n+1} \to \mathbb{R}$ is the rate of change of the variable $\boldsymbol{x}_i$, and $\boldsymbol{x}_i^0 \in \mathbb{R}$ is the initial condition at time t_0.

Theorem 2.1.1 (Existence and uniqueness theorem)**.** *Consider the initial value problem defined in Equation* (2.1.1)*. Suppose that each function F_i and its partial derivatives $\frac{\partial F_i}{\partial x_j}$ for $i, j = 1, \ldots, n$ are continuous in a region $R \subset \mathbb{R}^{n+1}$ defined by*

$$\alpha < t < \beta, \quad \alpha_1 < x_1 < \beta_1, \quad \ldots, \quad \alpha_n < x_n < \beta_n,$$

and that the initial point $(t_0, x_1^0, \ldots, x_n^0) \in R$. Then there exists a time interval $|t - t_0| < h$, for some $h > 0$, over which a unique solution $x_i = \phi_i(t)$ exists and

satisfies the initial condition for all $i = 1, \ldots, n$.

2.1.1 Equilibria and stability

An *equilibrium point* $\boldsymbol{x}^* \in \mathbb{R}^n$ of an autonomous system

$$\dot{\boldsymbol{x}} = f(\boldsymbol{x})$$

is a point at which the system remains constant over time, i.e., $f(\boldsymbol{x}^*) = \mathbf{0}$. In the context of infectious disease modelling, such points often represent disease-free or endemic steady states, and analyzing their stability helps determine whether the system will tend to or away from such states under small perturbations.

An equilibrium point $\boldsymbol{x}^*$ is said to be locally asymptotically stable if solutions that start sufficiently close to $\boldsymbol{x}^*$ not only remain close for all time but also converge to it as $t \to \infty$. Mathematically, there exists a neighbourhood U of $\boldsymbol{x}^*$ such that for any initial condition $\boldsymbol{x}_0 \in U$, the solution $\boldsymbol{x}(t) \to \boldsymbol{x}^*$ as $t \to \infty$.

The stability of $\boldsymbol{x}^*$ can be assessed using the Jacobian matrix $J(\boldsymbol{x}) = Df(\boldsymbol{x})$, evaluated at the equilibrium. If all eigenvalues of $J(\boldsymbol{x}^*)$ have strictly negative real parts, then $\boldsymbol{x}^*$ is locally asymptotically stable. If any eigenvalue has a positive real part, the equilibrium is unstable. This linearization technique is widely used to study the local behaviour of nonlinear systems near equilibria.

An equilibrium point is said to be globally asymptotically stable (GAS) if it is both locally asymptotically stable and if, for every initial condition $\boldsymbol{x}_0 \in \mathbb{R}^n$, the solution $\boldsymbol{x}(t) \to \boldsymbol{x}^*$ as $t \to \infty$. Establishing GAS typically requires the construction of a suitable Lyapunov function or the use of global analytical methods. In epidemiological models, a GAS disease-free equilibrium implies that the infection will die out regardless of the initial size of the infected population.

The stability of $\boldsymbol{x}^*$ can be assessed by analyzing the Jacobian matrix $J(\boldsymbol{x}) =$

$Df(\boldsymbol{x})$ evaluated at the equilibrium. If all the eigenvalues of $J(\boldsymbol{x}^*)$ have strictly negative real parts, then $\boldsymbol{x}^*$ is locally asymptotically stable. If any eigenvalue has a positive real part, the equilibrium is unstable. This linearization method provides a powerful tool for determining the behaviour of nonlinear systems near equilibria.

2.2 Epidemiological models and stability of the disease-free equilibrium

In mathematical epidemiology, compartmental models are typically formulated as systems of ODEs in $\mathbb{R}^n_+$ (since population numbers are non-negative). We consider a compartmental disease transmission model in $\mathbb{R}^n_+$ described by the following system of ordinary differential equations:

$$\dot{\boldsymbol{x}} = \boldsymbol{f}(\boldsymbol{x}) = \mathcal{F}(\boldsymbol{x}) - \mathcal{V}(\boldsymbol{x}), \tag{2.2.1}$$

where:

- $\boldsymbol{x} = (x_1, \ldots, x_n)^\top \in \mathbb{R}^n_+$ represents the state vector, with each $x_i \geqslant 0$ denoting the number of individuals in compartment i
- The first m compartments $(x_1, \ldots, x_m)$ correspond to infected individuals
- $\mathcal{F}(\boldsymbol{x}) = (\mathcal{F}_1(\boldsymbol{x}), \ldots, \mathcal{F}_n(\boldsymbol{x}))^\top$ is the vector of new infection rates
- $\mathcal{V}(\boldsymbol{x}) = (\mathcal{V}_1(\boldsymbol{x}), \ldots, \mathcal{V}_n(\boldsymbol{x}))^\top$ represents net transfer rates, where each component can be decomposed as:

  $$\mathcal{V}_i(\boldsymbol{x}) = \mathcal{V}_i^-(\boldsymbol{x}) - \mathcal{V}_i^+(\boldsymbol{x})$$

  with $\mathcal{V}_i^-$ being the outflow rate and $\mathcal{V}_i^+$ the inflow rate for compartment i

- The function $\boldsymbol{f}$ is continuously differentiable at least twice in each variable

(2.2.1) can be rewritten component-wise by splitting the state as $\boldsymbol{x} = (x_S, x_I)$, with the variables $\boldsymbol{x}_S \in \mathbb{R}_+^{n-m}$ and $\boldsymbol{x}_I \in \mathbb{R}_+^m$ representing the number of individuals in various compartments who are not infected and not transmitting the disease and the number of infected individuals, respectively. In this case, (2.2.1) takes the form

$$\dot{x}_S = \mathcal{F}_S(x) - \mathcal{V}_S(x) \tag{2.2.2a}$$

$$\dot{x}_I = \mathcal{F}_I(x) - \mathcal{V}_I(x), \tag{2.2.2b}$$

with $\mathcal{F}_S$, $\mathcal{F}_I$, $\mathcal{V}_S$ and $\mathcal{V}_I$ the corresponding components of $\mathcal{F}$ and $\mathcal{V}$.

We assume the existence of a Disease-Free Equilibrium (DFE) denoted as $\boldsymbol{x}^* = (\boldsymbol{x}_S^*, \mathbf{0})$, following the conditions established by van den Driessche and Watmough [31].

2.2.1 The basic reproduction number

The basic reproduction number is a crucial factor in studying infectious diseases as it determines whether the disease will fade away or spread in a population over time. It represents the number of secondary infections caused by one primary infection in a population where everyone is susceptible. If $\mathcal{R}_0 > 1$, it means that one primary infection can result in more than one secondary infection, leading to an unstable disease-free equilibrium and an outbreak of the epidemic. On the other hand, if $\mathcal{R}_0 < 1$, it implies that the situation is under control, and the disease-free equilibrium is locally stable, making it impossible for the disease to persist. Therefore, when dealing with a pandemic, it is crucial to develop an effective strategy to reduce the reproduction number to less than one as soon as possible [21].

To compute the basic reproduction number, we use the method of [31]. This involves assuming that (2.2.1) satisfies the following conditions:

(A1) Non-negativity: if $x \geqslant 0$, then $\mathcal{F}_i, \mathcal{V}_i^+, \mathcal{V}_i^- \geqslant 0$ for $i = 1, ..., n$.

(A2) No outflow from empty compartments: $\mathcal{V}_i^- = 0$ if $x = 0$.

(A3) Zero incidence of infection in uninfected compartments: $\mathcal{F}_i = 0$ for $i > m$.

(A4) Invariance of disease-free subspace: $\mathcal{F}_i(x) = 0$ and $\mathcal{V}_i^+(x) = 0$ for $i = 1, ..., m$ whenever $x \in \mathrm{X}_s$.

(A5) Eigenvalues at DFE are negative: If $\mathcal{F}(x)$ is set to zero, then all eigenvalues of the Jacobian matrix $Df(x_0)$ evaluated at a disease-free equilibrium (DFE) x_0 have negative real parts.

The basic reproduction number of (2.2.1) is then defined as $\mathcal{R}_0 = \rho(FV^{-1})$, where $\rho(\cdot)$ is the spectral radius of the next-generation matrix evaluated at the DFE x_0, i.e., the modulus of the largest eigenvalue of FV^{-1}.

2.2.2 Local asymptotic stability of the DFE

Using the computation method in the previous section, the following result then holds, which makes a further assumption on $\boldsymbol{x}_0$.

Theorem 2.2.1 ([31]). *If $\boldsymbol{x}_0$ is a locally stable DFE of the model* (2.2.1)*, then:*

- *x_0 is locally asymptotically stable if $\mathcal{R}_0 < 1$ (Small outbreaks die out and the population returns to the disease-free state)*
- *x_0 is unstable if $\mathcal{R}_0 > 1$ (Small outbreaks lead to an epidemic)*

2.2.3 Global stability of DFE

We represent the system (2.2.2) on the positively invariant set $\Omega \subset \mathbb{R}_+^{n_1+n_2}$ in its pseudo-triangular form:

$$\dot{\boldsymbol{x}}_S = \boldsymbol{T}_S(\boldsymbol{x})(\boldsymbol{x}_S - \boldsymbol{x}_S^*) + \boldsymbol{T}_{SI}(\boldsymbol{x})\boldsymbol{x}_I \tag{2.2.3a}$$

$$\dot{\boldsymbol{x}}_I = \boldsymbol{T}_I(\boldsymbol{x})\boldsymbol{x}_I \tag{2.2.3b}$$

where:

- $\boldsymbol{x} = (\boldsymbol{x}_S, \boldsymbol{x}_I) \in \mathbb{R}_+^{n_1} \times \mathbb{R}_+^{n_2}$ is the state vector partitioned into susceptible and infected compartments
- $\boldsymbol{x}_S^*$ is the susceptible components at the disease-free equilibrium
- The system matrices are decomposed by epidemiological mechanisms:

$$\boldsymbol{T}_S(\boldsymbol{x}) = \boldsymbol{M}_{SS}(\boldsymbol{x}) - \boldsymbol{D}_{SS}(\boldsymbol{x})$$
$$\boldsymbol{T}_{SI}(\boldsymbol{x}) = \boldsymbol{M}_{SI}(\boldsymbol{x}) - \boldsymbol{D}_{SI}(\boldsymbol{x})$$
$$\boldsymbol{T}_I(\boldsymbol{x}) = \boldsymbol{M}_{II}(\boldsymbol{x}) - \boldsymbol{D}_{II}(\boldsymbol{x})$$

  where $\boldsymbol{M}_{..}(\boldsymbol{x})$ matrices represent infection mechanisms and $\boldsymbol{D}_{..}(\boldsymbol{x})$ represent compartment transitions. Each matrix function is continuous on Ω and satisfies:

  - $\boldsymbol{M}_{SS}, \boldsymbol{D}_{SS} \in \mathbb{R}^{n_1 \times n_1}$: Dynamics within susceptible compartments
  - $\boldsymbol{M}_{SI}, \boldsymbol{D}_{SI} \in \mathbb{R}^{n_1 \times n_2}$: Infection generation from infected to susceptible
  - $\boldsymbol{M}_{II}, \boldsymbol{D}_{II} \in \mathbb{R}^{n_2 \times n_2}$: Transmission among infected compartments

Assume the following conditions hold:

H1 (Positivity and Dissipativity): System (2.2.3) is defined on a positively invariant set Ω of the nonnegative orthant (where all variables are non-negative). System (2.2.3) is dissipative within Ω, meaning trajectories are bounded as time goes to positive infinity.

H2 (Global Stability of Disease-free Subsystem): The subsystem of (2.2.3) representing disease dynamics in the absence of any disease (i.e., setting $\boldsymbol{x_I} = 0$) globally asymptotically stabilizes at the disease-free equilibrium on the projection of Ω onto the space of the first n_1 variables (representing the healthy population).

H3 (Metzler and Irreducibility of $\boldsymbol{T_I(x)}$): The matrix $\boldsymbol{T_I(x)}$, representing interactions within the infected population, is Metzler (all off-diagonal elements are non-negative) and irreducible (no isolated compartments) for any state $\boldsymbol{x}$ within Ω.

H4 (Upper Bound and Disease-free Equilibrium) There exists an upper bound matrix $\bar{\boldsymbol{T}}_{\boldsymbol{I}}$ for the set $\Re = \{\boldsymbol{T_I}(\boldsymbol{x}) / \boldsymbol{x} \in \Omega\}$ (i.e., every element of $\boldsymbol{T_I(x)}$ is less than or equal to the corresponding element in $\bar{\boldsymbol{T}}_{\boldsymbol{I}}$). This upper bound either does not belong to the original set $\Re$ or if it does (i.e., it's the maximum), then any state $\boldsymbol{x}$ in Ω where this maximum is achieved has its first n_1 components equal to zero (representing no disease).

H5 (Stability Modulus of Upper Bound): The spectral bound (greatest real part of the eigenvalues) of the upper bound matrix $\bar{\boldsymbol{T}}_{\boldsymbol{I}}$, denoted by $\alpha\left(\bar{\boldsymbol{T}}_{\boldsymbol{I}}\right)$, is less than or equal to zero.

Theorem 2.2.2 ([14])**.** *Under hypotheses (H1–H5), the disease-free equilibrium (DFE) of* (2.2.3) *is globally asymptotically stable within the set* Ω*.*

Corollary 2.2.3. *If hypotheses (H1–H5) hold for* (2.2.3) *and* $\bar{\boldsymbol{T}}_{\boldsymbol{I}} = \boldsymbol{T_I}(\boldsymbol{x}_{\boldsymbol{S}}^*, 0)$*, then the DFE is globally asymptotically stable if and only if* $\mathcal{R}_0 \leqslant 1$*.*

Proof. The Jacobian of the system at the DFE is

$$J = \begin{pmatrix} \boldsymbol{T_S}(\boldsymbol{x}_{\boldsymbol{S}}^*, 0) & \boldsymbol{T_{SI}}\left(\boldsymbol{x}_{\boldsymbol{S}}^*, 0\right) \\ 0 & \boldsymbol{T_I}\left(\boldsymbol{x}_{\boldsymbol{I}}^*, 0\right) \end{pmatrix}$$

Hence $\alpha\left(\bar{\boldsymbol{T}}_{\boldsymbol{I}}\right) \leqslant 0$ is a necessary condition. And this is equivalent to $\mathcal{R}_0 \leqslant 1$. □

2.3 Sensitivity analysis

Sensitivity analysis is an important step in understanding how model parameters influence the outcomes of infectious disease models. In this study, we performed a

global sensitivity analysis using the Partial Rank Correlation Coefficient (PRCC) method. This approach is well-suited for complex deterministic or stochastic models where the relationship between parameters and outcomes is not analytically tractable.

The PRCC method evaluates the strength and direction of the monotonic relationship between each input parameter and a selected model output—typically $\mathcal{R}_0$, prevalence, or final epidemic size—while controlling for the influence of other parameters. Unlike local methods (e.g., normalized forward sensitivity indices), PRCC does not require differentiability or an explicit functional form of the outcome variable.

To conduct the PRCC analysis, we generated a Latin Hypercube Sampling (LHS) of the parameter space, simulated the model outputs for each sample, and then computed the PRCC values using rank-transformed data. A high absolute PRCC value indicates a strong monotonic influence of the parameter on the outcome.

This method provides valuable insights into which parameters most strongly affect the transmission dynamics of the disease, thereby informing parameter prioritization and intervention strategies.

2.4 Continuous-time Markov chains (CTMC)

A continuous-time Markov chain (CTMC) is a stochastic process that models the evolution of a system over continuous time, where the future state depends only on the current state and not on the sequence of events that preceded it. This is known as the Markov property [22].

Let $\{X(t), t \geqslant 0\}$ be a CTMC with a countable state space $\mathcal{S}$. The process is characterized by transition rates q_{ij}, which denote the instantaneous rate at which the system transitions from state $i \in \mathcal{S}$ to state $j \in \mathcal{S}$ $(j \neq i)$. The matrix $Q = [q_{ij}]$ is called the infinitesimal generator matrix, and it satisfies the following properties:

- $q_{ij} \geqslant 0$ for $i \neq j$,
- $q_{ii} = -\sum_{j \neq i} q_{ij}$.

The holding time in each state i is exponentially distributed with rate $-q_{ii}$, and after this time elapses, the process jumps to a new state j with probability $\frac{q_{ij}}{-q_{ii}}$. This formulation makes CTMCs particularly well-suited for modelling biological processes, such as the transmission of infectious diseases, where state transitions (e.g., infection, recovery, colonization) occur randomly over continuous time.

In this thesis, CTMCs are used to represent the stochastic evolution of patient, healthcare worker, and environmental states in an intensive care unit (ICU) setting. The model includes a set of discrete states representing the compartmental status of individuals and transitions governed by probabilistic rates informed by biological and clinical parameters.

2.5 From ODE Models to CTMC Models

Deterministic models of infectious disease dynamics are commonly formulated using systems of ordinary differential equations (ODEs). In such models, the state variables represent population-level averages (e.g., the proportion of susceptible or infected individuals), and their evolution is governed by deterministic rates. For example, in a simple SIR model, the infection term βSI represents the expected number of new infections per unit time, where S and I denote the numbers of susceptible and infected individuals, respectively. These models are particularly useful for studying the average long-term behaviour of epidemics and for deriving threshold quantities such as the basic reproduction number $\mathcal{R}_0$.

However, ODE models implicitly assume that populations are very large and that transitions between compartments occur continuously and deterministically. In real-world healthcare settings, such as intensive care units (ICUs), the number of

patients, healthcare workers, and environmental sites is relatively small. Under these conditions, randomness in infection, recovery, and decontamination events becomes significant, and deterministic models may fail to capture the variability observed in practice.

To account for this intrinsic randomness, the ODE framework can be reformulated as a stochastic model using continous time Markov chains (CTMC). In this setting, the same transition mechanisms (e.g., infection, recovery, discharge) are retained, but they are expressed as random events occurring at specified rates. For instance, while the ODE model represents the infection rate as βSI, in the CTMC formulation, the number of infection events in a short time interval Δt follows a Poisson distribution with mean $\beta SI\Delta t$. Thus, instead of evolving deterministically, the system undergoes random jumps between discrete states, with the probability of each transition determined by the corresponding rate.

In summary, the ODE model describes the expected dynamics of the system, while the CTMC model captures both the expected behaviour and the stochastic fluctuations around it. This transition is particularly important in the context of nosocomial fungal infections, where small populations and rare events can significantly influence outbreak dynamics. In this thesis, we use CTMCs to provide a more realistic description of transmission dynamics in ICUs, complementing the insights gained from deterministic ODE analysis.

2.6 Nosocomial infections and *Candida auris*

Nosocomial infections, also known as hospital-acquired infections (HAIs), are infections acquired by patients during their stay in a healthcare setting, particularly in intensive care units (ICUs), where individuals are more vulnerable due to weakened immune systems and invasive medical procedures. These infections pose a significant

public health risk, contributing to prolonged hospital stays, increased mortality, and rising healthcare costs. Common types of HAIs include bloodstream infections, urinary tract infections, ventilator-associated pneumonia, and surgical site infections. Transmission pathways typically involve contact with contaminated healthcare workers (HCWs), medical equipment, and environmental surfaces.

C. auris is an emerging multidrug-resistant fungal pathogen of growing concern in nosocomial settings. Since its first identification in 2009, *C. auris* has been reported globally and has caused multiple hospital outbreaks. It is notoriously difficult to treat due to resistance to multiple classes of antifungal drugs and is also challenging to eradicate from hospital surfaces. Moreover, it is frequently misidentified by standard laboratory methods, which can delay appropriate clinical responses and infection control measures.

In ICU settings, *C. auris* poses particular risk due to its ability to persist on surfaces and skin, its transmission via both direct (e.g., through HCWs) and indirect (e.g., via the environment) contact, and the high mortality rates associated with invasive infections. Therefore, effective infection prevention and control require a thorough understanding of its biological characteristics and transmission pathways.

2.7 Mathematical modelling of nosocomial pathogens

Mathematical models have played a pivotal role in enhancing our understanding of nosocomial transmission dynamics and evaluating infection control strategies. Traditional models often use compartmental frameworks based on systems of ordinary differential equations (ODEs) to describe the progression of individuals through various epidemiological states (e.g., susceptible, colonized, infected).

One of the earliest such models is that of Austin et al. [4], who developed a dynamic transmission model to study the spread of antibiotic-resistant bacteria in

hospitals. Their work incorporated patient movement and HCW contact patterns, laying the foundation for many subsequent models. Barnes et al. [5] extended this approach by integrating environmental decontamination and hand hygiene compliance in the context of *Clostridium difficile* control.

Other works have used agent-based models (ABMs) and stochastic frameworks to account for individual-level variability and randomness in transmission events [20, 28]. These approaches are particularly useful in modelling small populations such as ICU wards, where stochasticity plays a critical role.

While the majority of early models focused on bacterial infections, recent efforts have shifted toward fungal pathogens, including *C. auris*. For example, Welsh et al. [33] proposed a stochastic compartmental model incorporating colonization, environmental persistence, and delayed detection to study *C. auris* outbreaks. These models typically emphasize indirect transmission pathways, asymptomatic carriers, and long environmental survival times—features especially relevant to fungal pathogens.

Such modelling frameworks provide essential insight into how various factors—e.g., screening, isolation, decontamination, and antifungal management can influence outbreak dynamics and control efforts. The model developed in this thesis builds upon this body of work by incorporating both deterministic and stochastic elements to study transmission in ICU environments, with a specific focus on the roles of HCWs and the environment in spreading *C. auris*.

3

Model assumptions and formulation

In this chapter, we present a mathematical model to show the intricate dynamics underpinning nosocomial fungal infections within the confines of Intensive Care Units (ICUs), encompassing both environmental transmission vectors and the involvement of healthcare personnel.

Consider an intensive care unit (ICU) comprising patients and healthcare workers. We categorize patients in this critical care unit into six distinct groups, based on the stage of their fungal infection and the results of their diagnostic tests. These categories are Susceptible Uncolonized (P_S), Colonized (P_C), Dectected Infectious (I_D) or Undetected Infectious (I_U), Recovered Colonized (R_C) and Dead ("morts" in French) (M). The remainder of the population consists of healthcare workers (HCWs). It is assumed that HCWs act as "vectors" of the disease: they can carry it from patient to patient if they become colonized during a healthcare act, but do not go on to develop an infection with the disease itself. The number of uncontaminated susceptible HCWs is denoted H_S, while those bearing the pathogen are denoted H_C. Finally, the pathogen can also contaminate the environment; the concentration of

fungal pathogens in the ICU environment is denoted by E_C. The state variables used are summarised in Table 3.1.

Table 3.1: Variables used in (3.2.1). HCW: health care worker.

Variable	Meaning
P_S	Uncolonized susceptible patient
P_C	Colonized patient
I_D	Identified/detected colonized patient
I_U	Unidentified/undetected colonized patient
R_C	Recovered colonized patient
M	Fungal-induced death
H_S	Uncontaminated susceptible HCW
H_C	Contaminated HCW
E_C	Contaminated environment

3.1 Model assumptions

We make the following assumptions:

1. Patients are admitted into the ICU at a constant rate b_P. It is assumed that they are tested upon entry and are therefore admitted in an uncolonized state. They are discharged from the facility at a *per capita* discharge rate d_P.

2. Healthcare workers are recruited at a constant rate b_H and leave the facility at the *per capita* rate d_H. Recruitment and discharge rates of HCW are typically chosen to account for work periods, meaning these rates are quite high.

3. Fungal infection is transmitted by colonized, detected and undetected infectious patients to uncontaminated healthcare workers at rates β_C, β_D and β_U, respectively. Infection is transmitted by contaminated HCWs to uncolonized susceptible patients at the rate β_H. We do assume that there is no patient-to-patient transmission.

4. The ICU environment is contaminated by fungal pathogens, when colonized, detected and undetected infectious patients contaminate at rates ψ_C, ψ_D and ψ_U, respectively. The environment in turn contaminates uncolonized patients indirectly at a rate β_E. It is assumed that HCW take precautionary measures and are therefore not contaminated by the environment.

5. An exponentially distributed period of latency of average length $1/\varepsilon$ days is assumed to occur after colonization of a patient and prior to the development of an associated infection. Since HCWs are vectors, they do not develop infection this way.

6. A patient takes an average $1/\gamma_D$ days to recover after colonization.

7. After recovering from mycosis, patients develop temporary immunity lasting on average $1/\tau_R$ days.

8. The *per capita* rates of disease-induced death because of infection by *C. auris* are δ_C, δ_D, and δ_U for colonized, detected, and undetected patients, respectively.

9. Contaminated healthcare workers are decontaminated at a rate μ_H, an outcome of employing disinfectants for hand hygiene. It is assumed that after their shift and before their shift, HCWs go through thorough sanitation and thus do not remain contaminated from one shift to the next.

10. An (exponentially distributed) average viable period of $1/\mu_E$ days is assumed for the *C. auris* pathogen in the environment. This encodes resistance to common disinfecting agents, which are assumed to be used regularly in a hospital environment.

11. The probability of misidentifying *C. auris* in standard medical laboratories is known to be relatively high [8, 18]. We define ϕ as the fraction of colonized or

infected patients identified as having *C. auris*. Patients who are not correctly identified due to diagnostic limitations are classified as Misidentified Infected (I_U).

A flow diagram of the nosocomial fungal infections model is shown in Figure 3.1.

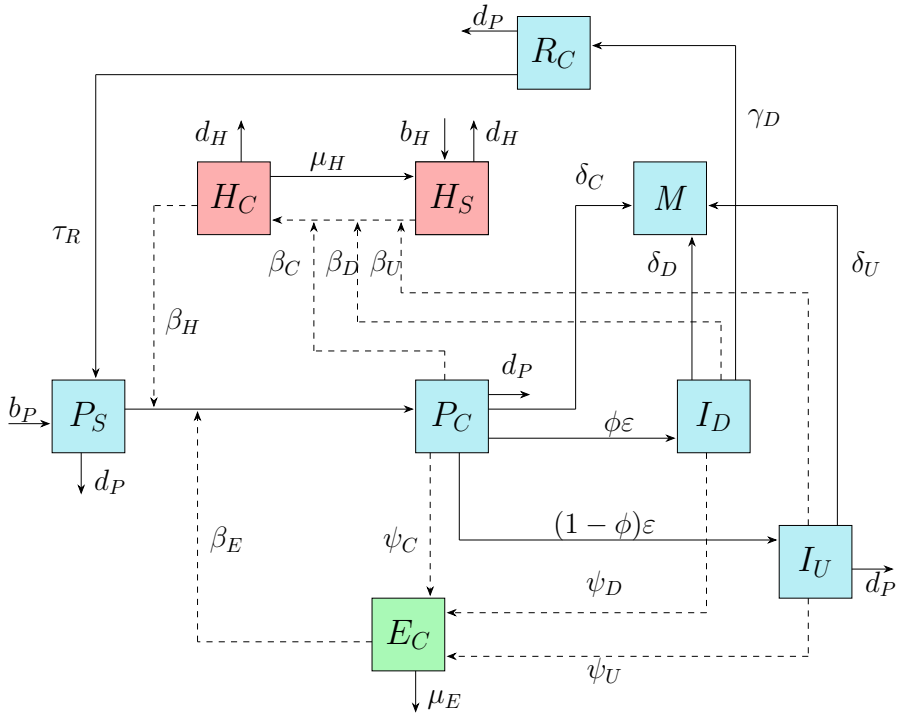

Figure 3.1: Flow diagram of nosocomial fungal infection.

3.2 ODE model equations

Let us assume the state of the system at any time t is represented by the vector

$$\boldsymbol{X}(t) = (P_S(t), P_C(t), I_D(t), I_U(t), R_C(t), H_S(t), H_C(t), E_C(t), M(t)),$$

where each component represents the population in different compartments at time t. As is customary, we ignore time dependence if this does not lead to confusion. Then based on the assumptions above, the model for nosocomial fungal infections in

healthcare settings takes the form below.

$$\dot{P}_S = b_P + \tau_R R_C - (\beta_H H_C + \beta_E E_C) P_S - d_P P_S \tag{3.2.1a}$$

$$\dot{P}_C = (\beta_H H_C + \beta_E E_C) P_S - \varepsilon P_C - \delta_C P_C - d_P P_C \tag{3.2.1b}$$

$$\dot{I}_D = \phi \varepsilon P_C - \gamma_D I_D - \delta_D I_D \tag{3.2.1c}$$

$$\dot{I}_U = (1 - \phi)\, \varepsilon P_C - \delta_U I_U - d_P I_U \tag{3.2.1d}$$

$$\dot{R}_C = \gamma_D I_D - \tau_R R_C - d_P R_C \tag{3.2.1e}$$

$$\dot{H}_S = b_H + \mu_H H_C - (\beta_C P_C + \beta_D I_D + \beta_U I_U) H_S - d_H H_S \tag{3.2.1f}$$

$$\dot{H}_C = (\beta_C P_C + \beta_D I_D + \beta_U I_U) H_S - \mu_H H_C - d_H H_C \tag{3.2.1g}$$

$$\dot{E}_C = \psi_C P_C + \psi_D I_D + \psi_U I_U - \mu_E E_C \tag{3.2.1h}$$

We also include a compartment for counting deaths,

$$\dot{M} = \delta_C P_C + \delta_D I_D + \delta_U I_U. \tag{3.2.1i}$$

The model is considered with nonnegative initial conditions. A list of the parameters used in (3.2.1), their meaning and units is given in Table 3.2.

3.3 Continuous-time Markov chain model

We also consider a continuous-time Markov chain (CTMC) analogue of (3.2.1). This stochastic model complements the ODE model in that it incorporates random fluctuations that arise from the stochastic nature of the transmission process and, perhaps even more importantly, makes accounting for the events occurring in the system much easier. CTMCs are also much better suited at handling low population counts than are ODE.

Table 3.2: Parameters of (3.2.1), where "pop" stands for population.

Parameter	Definition	Unit
	Demography	
b_P	Patient admission rate to ICUs	pop.day^{-1}
d_P	Discharge rate of patients	day^{-1}
b_H	HCW recruitment rate for hospital	pop.day^{-1}
d_H	HCW discharge rate	day^{-1}
	Pathogen transmission	
β_H	Contaminated HCWs to uncolonized patients	(pop.day)$^{-1}$
β_E	Contaminated environment to uncolonized patients	(cell.day)$^{-1}$
β_C	Colonized patients to uncontaminated HCWs	(pop.day)$^{-1}$
β_D	Identified infectious patients to uncontaminated HCWs	(pop.day)$^{-1}$
β_U	Unidentified infectious patients to uncontaminated HCWs	(pop.day)$^{-1}$
	Disease characteristics	
$1/\varepsilon$	Average duration of latent period	day
$1/\gamma_D$	Average time to recovery from fungal infection	day
$1/\tau_R$	Average duration of immunity to fungal reinfection	day
ϕ	Fraction of infectious patients detected	–
δ_C	Fungal-induced death rate of P_C	day^{-1}
δ_D	Fungal-induced death rate of I_D	day^{-1}
δ_U	Fungal-induced death rate of I_U	day^{-1}
μ_H	HCW decontamination rate	day^{-1}
μ_E	Environmental fungal decay rate	day^{-1}
	Fungal release into the environment	
ψ_C	By colonized patients	cell.(pop.day)$^{-1}$
ψ_D	By detected infectious patients	cell.(pop.day)$^{-1}$
ψ_U	By undetected infectious patients	cell.(pop.day)$^{-1}$

Informed by the structure of the deterministic model, we construct the CTMC $\boldsymbol{X}(t)$. The state space of the CTMC is the set of all possible population distributions among these compartments and the system evolves through transitions between these states at random times. The infinitesimal transition probability from state i to state j is given by

$$p_{i,j}(\Delta t) = \mathbb{P}\{\boldsymbol{X}(t+\Delta t) = j | \boldsymbol{X}(t) = i\} = \rho(i,j)\,\Delta t + o(\Delta t), \tag{3.3.1}$$

where $\rho(i,j)$ is the transition rate associated with the transition from state i to state j [3, 22]. This transition rate depends on the current state of the system and parameters of the model. The chain is homogeneous since parameters are constant through time. Note also that there is no distribution of probability associated to parameter values. Possible transitions and their corresponding rates are summarized in Table 3.3.

Table 3.3: State transitions and rates for the CTMC (3.3.1).

Transition	Type of event	Weight
$P_S \to P_S + 1$	Admission of a P_S	b_P
$P_S \to P_S - 1$	Discharge of a P_S	$d_P P_S$
$P_C \to P_C - 1$	Discharge of a P_C	$d_P P_C$
$I_U \to I_U - 1$	Discharge of an I_U	$d_P I_U$
$R_C \to R_C - 1$	Discharge of a R_C	$d_P R_C$
$H_S \to H_S + 1$	Start of shift of a H_S	b_H
$H_S \to H_S - 1$	End of shift of a H_S	$d_H H_S$
$H_C \to H_C - 1$	End of shift of a H_C	$d_H H_C$
$(P_S, P_C) \to (P_S - 1, P_C + 1)$	H_C infects P_S	$\beta_H H_C P_S$
$(P_S, P_C) \to (P_S - 1, P_C + 1)$	E_C infects P_S	$\beta_E E_C P_S$
$(H_S, H_C) \to (H_S - 1, H_C + 1)$	P_C infects H_S	$\beta_C P_C H_S$
$(H_S, H_C) \to (H_S - 1, H_C + 1)$	I_D infects H_S	$\beta_D I_D H_S$
$(H_S, H_C) \to (H_S - 1, H_C + 1)$	I_U infects H_S	$\beta_U I_U H_S$
$(P_C, I_D) \to (P_C - 1, I_D + 1)$	Detection after end of latency	$\phi\varepsilon P_C$
$(P_C, I_U) \to (P_C - 1, I_U + 1)$	No detection after end of latency	$(1-\phi)\,\varepsilon P_C$
$(I_D, R_C) \to (I_D - 1, R_C + 1)$	Recovery of I_D	$\gamma_D I_D$
$(R_C, P_S) \to (R_C - 1, P_S + 1)$	Waning of immunity for R_C	$\tau_R R_C$
$(P_C, M) \to (P_C - 1, M + 1)$	Death P_C because of disease	$\delta_C P_C$
$(I_D, M) \to (I_D - 1, M + 1)$	Death I_D because of disease	$\delta_D I_D$
$(I_U, M) \to (I_U - 1, M + 1)$	Death I_U because of disease	$\delta_U I_U$
$(H_C, H_S) \to (H_C - 1, H_S + 1)$	Waning of H_C	$\mu_H H_C$
$E_C \to E_C - 1$	Decay of pathogen	$\mu_E E_C$
$E_C \to E_C + 1$	Contamination of E_C by P_C	$\psi_C P_C$
$E_C \to E_C + 1$	Contamination of E_C by I_D	$\psi_D I_D$
$E_C \to E_C + 1$	Contamination of E_C by I_U	$\psi_U I_U$

4

Mathematical analysis

In this chapter, we analyze the dynamics of the general model (3.2.1). We analyze the positive invariant set and boundedness, as well as the existence, and uniqueness of the equilibrium. We also provide the basic reproduction number, local and global stability of the disease-free equilibrium point of (3.2.1).

4.1 Positivity and boundedness

Denote $\boldsymbol{X}(t)$ the solution of (3.2.1). The following result is useful later.

Proposition 4.1.1. *Assume that* $\boldsymbol{X}(0) \in \mathbb{R}^9_+$. *Then solutions to* (3.2.1) *satisfy* $\boldsymbol{X}(t) \in \mathbb{R}^9_+$ *for all* $t \geqslant 0$ *and are bounded.*

Proof. The proof of invariance of $\mathbb{R}^9_+$ under the flow of (3.2.1) is straightforward and is omitted. To prove boundedness, let $P(t) = P_S(t) + P_C(t) + I_D(t) + I_U(t) + R_C(t) + M(t)$ and $H(t) = H_S(t) + H_C(t)$. Then from (3.2.1a)-(3.2.1d) and (3.2.1i), we obtain

$$\dot{P} = b_P - d_P(P_S + P_C + I_U + R_C) \implies \dot{P} + d_P P \leqslant b_P.$$

Solving this differential inequality, we get

$$0 < P\left(t\right) \leqslant \frac{b_P}{d_P} + \left(P_0 - \frac{b_P}{d_P}\right) e^{-d_P t}, \tag{4.1.1}$$

where P_0 is the initial condition, and the left inequality follows from the invariance of $\mathbb{R}^9_+$.

We distinguish two cases:

- If $P_0 > b_P/d_P$, then $P(t)$ decreases monotonically towards b_P/d_P with $P(t) \geqslant b_P/d_P$ for all $t \geqslant 0$.
- If $P_0 < b_P/d_P$, then $P(t)$ increases monotonically towards b_P/d_P with $P(t) \leqslant b_P/d_P$ for all $t \geqslant 0$.

In both cases, $\lim_{t\to\infty} P(t) = b_P/d_P$.

Proceeding the same way, from (3.2.1f) and (3.2.1g), we get

$$0 < H\left(t\right) = \frac{b_H}{d_H} + \left(H_0 - \frac{b_H}{d_H}\right) e^{-d_H t},$$

where H_0 is the initial condition. Thus, $\lim_{t\to\infty} H(t) = b_H/d_H$, with the convergence being monotonic from above or below depending on H_0.

Now, let $\psi = \max\left(\psi_C, \psi_D, \psi_U\right)$. Then using (4.1.1) with t approaching infinity in (3.2.1h), we have

$$\dot{E}_C \leqslant \psi\left(P_C + I_D + I_U\right) - \mu_E E_C \implies \dot{E}_C + \mu_E E_C \leqslant \frac{\psi b_P}{d_P}.$$

Solving the differential inequality, we get

$$0 < E_C\left(t\right) \leqslant \frac{\psi b_P}{\mu_E d_P} + \left(E_{C0} - \frac{\psi b_P}{\mu_E d_P}\right) e^{-\mu_E t},$$

where $E_{C0} = E_C(0)$ is the initial condition. Thus, $\lim_{t\to\infty} E_C(t) = \psi b_P/(\mu_E d_P)$, with

the convergence being monotonic from above or below depending on E_{C0}.

Since $\boldsymbol{X}(0) \in \mathbb{R}^9_+$, all state variables are non-negative and the total population size is constant, each state variable must be bounded, which means that solutions to (3.2.1) are bounded. □

From the above result, we deduce that (3.2.1) is epidemiologically well-posed.

4.2 Disease-free equilibria

It is straightforward to verify that, in the absence of the infectious agent (i.e., $P_C = I_D = I_U = H_C = E_C = 0$), system (3.2.1) possesses a unique disease-free equilibrium (DFE):

$$\boldsymbol{E}_0 = \left(\frac{b_P}{d_P}, 0, 0, 0, 0, \frac{b_H}{d_H}, 0, 0, 0\right).$$

4.3 Basic reproduction number

To further study the transmission dynamics, we compute the basic reproduction number $\mathcal{R}_0$ of (3.2.1). This scalar value indicates the average number of secondary infections produced by a single infected individual in a fully susceptible population, with $\mathcal{R}_0 < 1$ implying disease extinction and $\mathcal{R}_0 > 1$ suggesting potential disease persistence. Let $\mathcal{I} = (P_C, I_D, I_U, H_C, E_C)$ denote the infected compartments. Following the next-generation matrix approach, we define $\mathcal{F}$ as the rate of appearance of new infections in $\mathcal{I}$ and $\mathcal{V}$ as the rate of transfer of individuals into and out of $\mathcal{I}$ by other processes, both evaluated at $\boldsymbol{E}_0$.

Under the assumption that patients (P_C, I_D, and I_U) fungal residue into the environment does not constitute a source of new infections, the next-generation matrix is derived as follows.

The matrices $\mathcal{F}$ and $\mathcal{V}$ are:

$$\mathcal{F} = \begin{pmatrix} (\beta_H H_C + \beta_E E_C) P_S \\ 0 \\ 0 \\ (\beta_C P_C + \beta_D I_D + \beta_U I_U) H_S \\ 0 \end{pmatrix} \quad \text{and} \quad \mathcal{V} = \begin{pmatrix} (\varepsilon + \delta_C + d_P)\, P_C \\ (\gamma_D + \delta_D) I_D - \phi \varepsilon P_C \\ (\delta_U + d_P) I_U - (1-\phi)\, \varepsilon P_C \\ (\mu_H + d_H) H_C \\ \mu_E E_C - \psi_C P_C - \psi_D I_D - \psi_U I_U \end{pmatrix}.$$

At the DFE $\boldsymbol{E}_0$, where $P_S^* = b_P/d_P$ and $H_S^* = b_H/d_H$, the Jacobian matrices $F = D\mathcal{F}(\boldsymbol{E}_0)$ and $V = D\mathcal{V}(\boldsymbol{E}_0)$ yield the next generation matrix:

$$FV^{-1} = \begin{pmatrix} [FV^{-1}]_{11} & [FV^{-1}]_{12} & [FV^{-1}]_{13} & [FV^{-1}]_{14} & [FV^{-1}]_{15} \\ 0 & 0 & 0 & 0 & 0 \\ 0 & 0 & 0 & 0 & 0 \\ [FV^{-1}]_{41} & [FV^{-1}]_{42} & [FV^{-1}]_{43} & 0 & 0 \\ 0 & 0 & 0 & 0 & 0 \end{pmatrix},$$

where each $[FV^{-1}]_{ij}$ represents the expected secondary infections in compartment i from one individual in compartment j at DFE. The basic reproduction number $\mathcal{R}_0$ is defined as the spectral radius of FV^{-1} i.e. $\mathcal{R}_0 = \rho(FV^{-1})$.

Due to the structure of FV^{-1}, we find two nonzero eigenvalues,

$$-\frac{\sqrt{4[FV^{-1}]_{14}[FV^{-1}]_{41} + [FV^{-1}]_{11}^2} - [FV^{-1}]_{11}}{2}$$

and

$$\frac{\sqrt{4[FV^{-1}]_{14}[FV^{-1}]_{41} + [FV^{-1}]_{11}^2} + [FV^{-1}]_{11}}{2}.$$

As the entries of FV^{-1} are nonnegative by construction, it follows that the basic

reproduction number is given by

$$\mathcal{R}_0 = \frac{\sqrt{4[FV^{-1}]_{14}[FV^{-1}]_{41} + [FV^{-1}]_{11}^2} + [FV^{-1}]_{11}}{2}.$$

where

$$\begin{aligned}
[FV^{-1}]_{11} &= \frac{b_P\beta_E}{d_P\mu_E}\left(\frac{\varepsilon\phi\psi_D}{(d_P+\delta_C+\varepsilon)(\delta_D+\gamma_D)} + \frac{\varepsilon(1-\phi)\psi_U}{(d_P+\delta_C+\varepsilon)(d_P+\delta_U)}\right.\\
&\qquad \left. + \frac{\psi_C}{d_P+\delta_C+\varepsilon}\right)\\
[FV^{-1}]_{14} &= \frac{b_P\beta_H}{d_P(\mu_H+d_H)}\\
[FV^{-1}]_{41} &= \frac{b_H\beta_U\varepsilon(1-\phi)}{d_H(d_P+\delta_C+\varepsilon)(d_P+\delta_U)} + \frac{b_H\beta_D\varepsilon\phi}{d_H(d_P+\delta_C+\varepsilon)(\gamma_D+\delta_D)}\\
&\qquad + \frac{b_H\beta_C}{d_H(d_P+\delta_C+\varepsilon)}
\end{aligned}$$

Remark: An explicit expression for $\mathcal{R}_0$ can easily be obtained using a symbolic computation software. However, this expression is really long and not really informative. In numerical work, we use the matrices F and V^{-1} and compute the spectral radius of FV^{-1}, or compute the expression above numerically.

4.4 Stability analysis

Proposition 4.4.1. *The disease-free equlibrium* $\boldsymbol{E}_0$ *of* (3.2.1) *is locally asymptotically stable in* $\mathbb{R}^9_+$ *if* $\mathcal{R}_0 < 1$ *and unstable in if* $\mathcal{R}_0 > 1$.

Proof. The Jacobian matrix of (3.2.1) at the disease-free state:

$$J = \begin{pmatrix} -\mathrm{d_P} & \tau_R & 0\\ 0 & -(\tau_R+\mathrm{d_P}) & 0\\ 0 & 0 & -d_H \end{pmatrix}$$

The matrix J is in lower triangular form, and its eigenvalues are the diagonal elements:

$$\lambda_1 = -\mathrm{d_P} < 0,\ \lambda_2 = -(\tau_R + \mathrm{d_P}) < 0,\ \lambda_3 = -d_H < 0$$

Since all eigenvalues are strictly negative, according to [31] (Theorem 2) we can conclude that the DFE for (3.2.1) is locally asymptotically stable if $\mathcal{R}_0 < 1$. Conversely, if $\mathcal{R}_0 > 1$, the DFE is unstable. □

Proposition 4.4.2. *The disease-free equilibrium* $\boldsymbol{E}_0$ *of* (3.2.1) *is globally asymptotically stable in* $\mathbb{R}^9_+$ *if* $\mathcal{R}_0 \leqslant 1$.

Proof. The proof uses the method in [14]. We set $\boldsymbol{x_S} = (P_S, R_C, M, H_S)$ and $\boldsymbol{x_I} = (P_C, I_D, I_U, H_C, E_C)$, where the domain is $\mathbb{R}^9_+$. This compact set is positively invariant (Proposition 4.1.1). We express the sub-system as $\dot{\boldsymbol{x}}_{\boldsymbol{S}} = T_{SS}\left(\boldsymbol{x_S}, 0\right)\left(\boldsymbol{x_S} - \boldsymbol{x}^*_{\boldsymbol{S}}\right)$, which gives:

$$\dot{P}_S = b_P + \tau_R R_C - d_P P_S \tag{4.4.1a}$$

$$\dot{R}_C = -\left(\tau_R + d_P\right) R_C \tag{4.4.1b}$$

$$\dot{M} = 0 \tag{4.4.1c}$$

$$\dot{H}_S = b_H - d_H H_S \tag{4.4.1d}$$

The system (4.4.1a)–(4.4.1b) is a nonhomogeneous linear system,

$$\begin{pmatrix} \dot{P}_S \\ \dot{R}_C \end{pmatrix} = \begin{pmatrix} -d_P & \tau_R \\ 0 & -(\tau_R + d_P) \end{pmatrix} \begin{pmatrix} P_S \\ R_C \end{pmatrix} + \begin{pmatrix} b_P \\ 0 \end{pmatrix}.$$

This upper triangular matrix is invertible and has two negative eigenvalues. As a consequence, $P_S(t), R_C(t)$ converges to a positive equilibrium. Furthermore, $M(t) = M_0$ for all $t > 0$. Finally, considering (4.4.1d), it is clear that $H_S(t) \to b_H/d_H$ as $t \to \infty$.

This confirms that the linear system (4.4.1) is (globally) asymptotically stable at the DFE $\boldsymbol{E}_0$, satisfying hypotheses H_1 and H_2 of [14].

Next, consider the infection-related matrix $T_{II}(x)$, given by

$$T_{II}(x) = \begin{pmatrix} -(\varepsilon + \delta_C + d_P) & 0 & 0 & \beta_H P_S & \beta_E P_S \\ \phi\varepsilon & -(\gamma_D + \delta_D) & 0 & 0 & 0 \\ (1-\phi)\,\varepsilon & 0 & -(\delta_U + d_P) & 0 & 0 \\ \beta_C H_S & \beta_D H_S & \beta_U H_S & -(\mu_H + d_H) & 0 \\ \psi_C & \psi_D & \psi_U & 0 & -\mu_E \end{pmatrix}$$

This matrix is irreducible for all $x \in \mathbb{R}^9_+$, thus satisfying hypothesis H_3.

To verify hypothesis H_4, observe that the maximum spectral radius is uniquely attained at the DFE $\mathbf{E}_0$. The corresponding Jacobian block at the DFE, denoted J_2, is:

$$J_2 = \begin{pmatrix} -(\varepsilon + \delta_C + d_P) & 0 & 0 & \beta_H \frac{b_P}{d_P} & \beta_E \frac{b_P}{d_P} \\ \phi\varepsilon & -(\gamma_D + \delta_D) & 0 & 0 & 0 \\ (1-\phi)\,\varepsilon & 0 & -(\delta_U + d_P) & 0 & 0 \\ \beta_C \frac{b_H}{d_H} & \beta_D \frac{b_H}{d_H} & \beta_U \frac{b_H}{d_H} & -(\mu_H + d_H) & 0 \\ \psi_C & \psi_D & \psi_U & 0 & -\mu_E \end{pmatrix}$$

This maximum is achieved only at $\mathbf{E}_0$, placing us within the setting of Corollary 4.4 from [14].

Finally, hypothesis H_5 requires that the spectral bound $\alpha(J_2) \leqslant 0$. Since J_2 is a Metzler matrix and is stable, this condition is fulfilled.

Having verified all five hypotheses H_1 through H_5, we conclude from Corollary 4.4 in [14] that the disease-free equilibrium $\mathbf{E}_0$ of system (3.2.1) is globally asymptotically stable in $\mathbb{R}^9_+$ if and only if $\mathcal{R}_0 \leqslant 1$. □

Note that we have not considered mathematically the case $\mathcal{R}_0 > 1$, since the computations are extremely complicated in this case. We suspect that the model goes to an endemic equilibrium and numerics seem to indicate that this is the case.

5

Computational analysis

This chapter presents a computational analysis of *Candida auris* transmission dynamics in an ICU setting conducted using deterministic and stochastic framework.

5.1 Parameter values and calculation methods

The parameters in Table 5.1 were derived from Canadian-specific data where available, with assumed values calibrated based on reasonable approximations and published literature.

Demographic parameters. The patient admission rate (b_P = 1–2 patients per day) was estimated using a typical ICU capacity of 10 beds and an average length of stay (LOS) of 3–7 days. This aligns with data from the Canadian Institute for Health Information (CIHI), which reports ICU-specific LOS values across Canadian provinces [12, 13]. This range yields admission rates consistent with full occupancy and realistic turnover in small-to-moderate capacity ICUs found in community and regional hospitals. The discharge rate (d_P) is modelled as the reciprocal of LOS, i.e., $1/d_P$ = 3–7 days.

The healthcare worker (HCW) recruitment rate (b_H = 30–60 per day) and dis-

charge rate (d_H = 2–4 per day) were assumed based on a three-shift daily schedule (8-hour shifts) and 10–20 HCWs active per shift. d_H was set to correspond with shift turnover, while b_H was scaled to maintain a stable HCW pool size.

Transmission and environmental parameters. The pathogen transmission rates ($\beta_H, \beta_C, \beta_D, \beta_U$) were informed by Methicillin-resistant Staphylococcus aureus (MRSA) modelling studies and scaled for fungal transmission in ICU settings [9]. Environmental contamination by colonized and infectious patients was modeled using pathogen release rates (ψ_C = 10–100, ψ_D = 5–50, and ψ_U = 20–200 cells/day), with higher rates assumed for undetected cases due to lack of isolation, consistent with findings from [26, 32]. Environmental decay of the fungal pathogen was modeled with $\mu_E = 1/10$–$1/20$ day^{-1}, reflecting surface viability of 10–20 days as documented in [1].

Disease progression and detection. The latency period from colonization to active infection was set as $1/\varepsilon$ = 10–30 days, based on data from ICU colonization studies that report median progression times of 14 days [6]. The recovery period was set at $1/\gamma_D$ = 10–20 days, while temporary immunity was modeled with $1/\tau_R$ = 30–100 days. The probability of correctly identifying colonized or infectious patients was modeled as ϕ = 0.5–0.7, accounting for high rates of misidentification in clinical laboratories [24, 29].

Mortality and decontamination. Mortality rates varied by patient type: colonized patients (δ_C) were assigned a very low risk ($1/\delta_C$ = 100–300 days), while detected infections ($1/\delta_D$ = 30–60 days) and undetected infections ($1/\delta_U$ = 15–30 days) were assigned progressively higher death rates to reflect lack of timely treatment [23]. The HCW decontamination rate (μ_H = 18–36 per day) was estimated from 6–12 hand hygiene events per shift over 3 shifts per day, consistent with World

Health Organization and CDC infection control guidelines [11, 25].

Table 5.1: Parameter values of (3.2.1). (For a more detailed parameter interpretation, see Table 3.2.)

Parameter	Definition	Range	Source
	Demography		
b_P	Patient admission rate to ICUs	1-2	[12]
$1/d_P$	Average patient stay before discharge	3-7	[13]
b_H	HCW recruitment rate for hospital	30-60	Assumed
d_H	HCW discharge rate	2-4	Assumed
	Disease transmission		
β_H	From contaminated HCWs to patients	0.05-0.2	[9]
β_E	From contaminated environment to patients	0.001 - 0.01	[1]
β_C	From colonized patients to HCWs	0.1-0.4	[9]
β_D	From detected infectious patients to HCWs	0.05-0.2	[9]
β_U	From undetected infectious patients to HCWs	0.1-0.4	[9]
	Disease characteristics		
$1/\varepsilon$	Average latent period	10-30	[6]
$1/\gamma_D$	Average recovery time	10-20	Assumed
$1/\tau_R$	Average immunity duration	30-100	Assumed
ϕ	Fraction of infectious patients detected	0.5-0.7	[24]
$1/\delta_C$	Time to death for P_C	100-300	Assumed
$1/\delta_D$	Time to death for I_D	30-60	[23]
$1/\delta_U$	Time to death for I_U	15-30	Assumed
μ_H	HCW decontamination rate	18-36	Assumed
$1/\mu_E$	Environmental survival time	10-20	[1]
	Fungal pathogen releasing into the environment		
ψ_C	By colonized patients	10-100	Assumed
ψ_D	By detected infectious patients	5-50	Assumed
ψ_U	By undetected infectious patients	20-200	[26, 32]

5.2 Parameter validation using CTMC

To ensure the realism of the parameter values and rates derived in Section 5.1, a continuous-time Markov chain (CTMC) is employed as an initial validation step prior to detailed numerical analysis. This approach verifies that the parameters yield

biologically plausible dynamics, particularly in the context of transmission dynamics initiated by a single colonized patient (P_C). The CTMC model corresponds to (3.2.1), with transition rates (summerised in Table 3.3.1) assumed to be constant, rendering the process homogeneous. Detailed derivations are omitted here; readers are referred to standard literature on the conversion of ordinary differential equations (ODEs) to CTMCs, such as [2].

The validation process begins by simulating the CTMC to assess the consistency of the rates with observed system behavior. Figure 5.1 illustrates two sample realizations: (5.1a) depicts the number of events per day for patients, and(5.1b) shows the corresponding dynamics for healthcare workers (HCWs). The events include various types such as admission, discharge, and shift changes, with rates summarized in the associated legend. These simulations utilize parameters derived in Section 5.1, starting from the DFE. Each scenario was simulated 1000 times, and results were averaged across replicates.

The results show patterns where event frequencies align with expected healthcare settings, suggesting plausible turnover rates. By placing this analysis early in the numerical section, we ensure that subsequent computations are grounded in parameters that reflect realistic system behaviour.

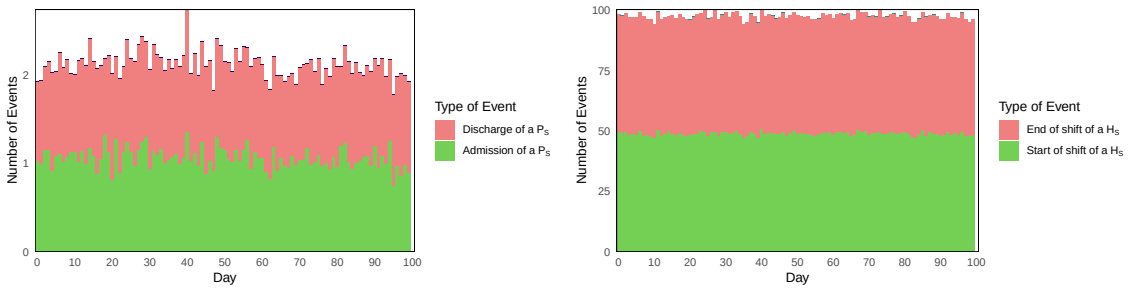

(a) Patients (b) HCWs

Figure 5.1: Number of events per day in the CTMC analogue of (3.2.1), initiated from the DFE. Results are averaged over 1000 stochastic simulations with parameters derived from Section 5.1. (a) Patients, showing daily events such as admission and discharge. (b) Healthcare workers (HCWs), showing daily event dynamics including shift changes.

5.3 Transmission pathways

To investigate the contributions of different infection routes to the overall transmission potential, we analyzed selected non-zero entries of the next-generation matrix FV^{-1} derived in Section 4.3. Although the full matrix contains eight potential pathways connecting patients (P_C, I_D, I_U), healthcare workers (H_C), and the environment (E_C), only three pathways contributed appreciably to the basic reproduction number $\mathcal{R}_0$ under the sampled parameter ranges: $P_C \to P_C$ (R_{11}), $H_C \to P_C$ (R_{14}), and $P_C \to H_C$ (R_{41}). We performed Monte Carlo simulations using 100,000 points in parameter space sampled from uniform distributions within biologically plausible ranges (Table 3.2). For each parameter set, the R_{ij} entries were computed analytically from FV^{-1}. We summarized the distribution of R_{ij} using boxplots (Figure 5.2), which capture both central tendencies and variability across the parameter space.

The results indicate that patient-to-patient transmission ($P_C \to P_C$) and HCW-to-patient transmission ($H_C \to P_C$) dominate, with median values around 14-15 and overlapping interquartile ranges. The $P_C \to P_C$ pathway represents an indirect reinforcement loop, whereby colonized patients amplify risk through secondary contacts and environmental contamination. In contrast, the $H_C \to P_C$ pathway reflects a direct route of transmission, where contaminated healthcare workers serve as immediate vectors between patients. Both mechanisms emerge as robust drivers of persistence.

By comparison, the pathway $P_C \to H_C$ (R_{41}) remains consistently close to zero, indicating that colonized patients rarely generate onward infections in healthcare workers in a manner that sustains transmission.

Overall, these findings emphasize that outbreak propagation is primarily shaped by the interaction of direct (HCW-mediated) and indirect (patient-reinforcing) transmission pathways, whereas other potential routes (e.g., involving the environment or infected patients) make negligible contributions under the considered parameter

ranges.

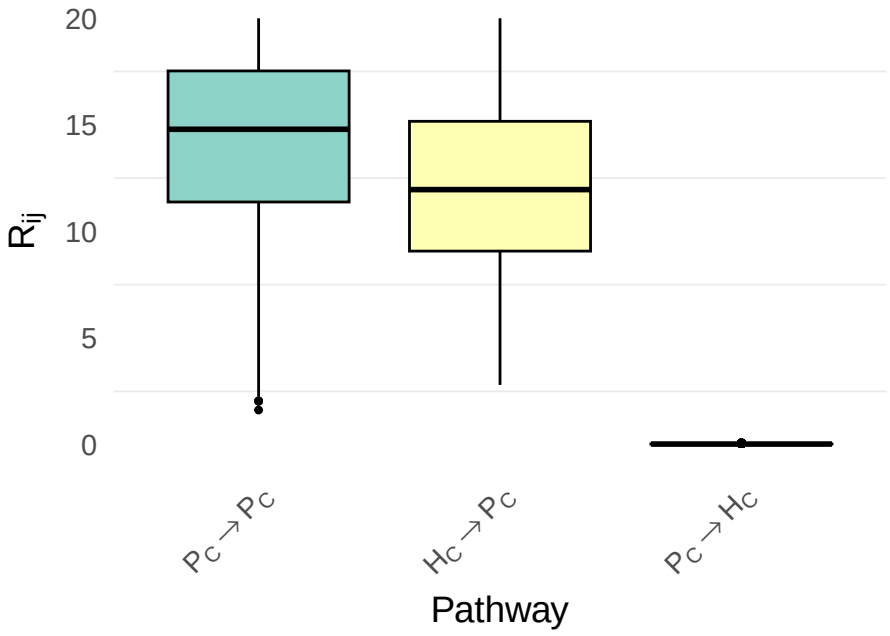

Figure 5.2: Distribution of non-negligible transmission pathway contributions (R_{ij}) from the next-generation matrix FV^{-1}, computed from 100,000 points in parameter space. Only three pathways, $P_C \rightarrow P_C$, $H_C \rightarrow P_C$, and $P_C \rightarrow H_C$, were retained for analysis, as the remaining five entries had negligible values. Pathways are labelled by source → target compartments, distinguishing between direct (HCW-mediated) and indirect (patient-reinforcing) transmission routes.

5.4 Sensitivity analysis

We performed a global sensitivity analysis to evaluate the influence of model parameters on the basic reproduction number $\mathcal{R}_0$ for *C. auris* transmission in an ICU setting. Using Sobol sampling, we generated 100,000 points in parameter space from uniform distributions based on the ranges in Table 5.1. The Sobol sequences were generated using the R package `qrng`, ensuring a low-discrepancy sampling approach for improved coverage of the parameter space. Partial Rank Correlation Coefficients (PRCCs) were computed using the `sensitivity` package with the `PCC` function, applying `furrr` for parallelization.

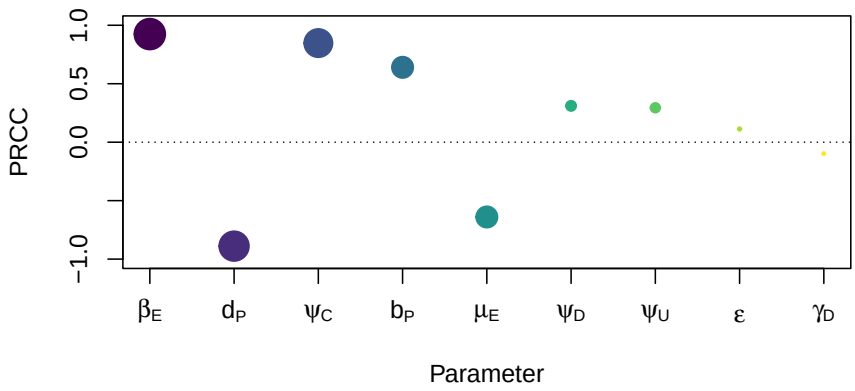

Figure 5.3: PRCC sensitivity indices of (3.2.1) obtained using Sobol sampling ($n = 100,000$ points in parameter space). The output shows that $\mathcal{R}_0$ is most strongly influenced by the environmental transmission rate (β_E) and fungal shedding from colonized patients (ψ_C), with patient discharge rate (d_P) having the strongest negative effect. Other parameters such as patient admission rate (b_P) and environmental fungal decay (μ_E) are moderately important, while HCW-related parameters have negligible impact.

The PRCC results are presented in Figure 5.3, identifying the primary drivers of $\mathcal{R}_0$. The environmental transmission rate (β_E, PRCC = 0.925) emerges as the most influential contributor to transmission, followed closely by environmental release from colonized patients (ψ_C, PRCC = 0.848), underscoring the central role of environmental contamination. The patient discharge rate (d_P, PRCC = -0.889) exhibits the strongest negative effect, reducing $\mathcal{R}_0$ by shortening the exposure time of susceptible patients in the ICU.

Other influential parameters include the patient admission rate (b_P, PRCC = 0.64), which increases $\mathcal{R}_0$ by introducing more susceptible individuals, and the environmental fungal decay rate (μ_E, PRCC = -0.64), which reduces transmission by decreasing environmental pathogen persistence. Fungal residue of detected (ψ_D, PRCC = 0.311) and undetected (ψ_U, PRCC = 0.294) patients also contribute moderately to transmission. The progression rate from colonization to infection (ε, PRCC

= 0.113) and recovery rate (γ_D, PRCC = -0.098) have relatively modest effects.

The remaining parameters – HCW-related transmission rates ($\beta_H, \beta_C, \beta_D, \beta_U$), HCW dynamics ($b_H, d_H$), decontamination rate (μ_H), detection probability (ϕ), and immunity waning rate (τ_R), have negligible influence on $\mathcal{R}_0$, with PRCC values close to zero. They are not shown in Figure 5.3.

These findings suggest that intervention strategies should prioritize environmental control, specifically by reducing environmental transmission (β_E) and enhancing fungal decay through cleaning and disinfection protocols (μ_E). Limiting fungal residue from colonized patients (ψ_C) and managing patient flow—by reducing ICU stay durations (d_P) or admissions (b_P)—also offer effective levers to suppress transmission. The minimal sensitivity of $\mathcal{R}_0$ to HCW-related parameters supports the interpretation that current infection control practices (e.g., hand hygiene) are likely sufficient to mitigate HCW-mediated spread, allowing resources to focus on high-impact environmental and patient turnover interventions.

5.5 Extinction dynamics across initial infection categories

We investigated extinction probabilities of *C. auris* outbreaks under different seeding scenarios using stochastic simulations of the CTMC model defined in (3.3.1). Both the basic reproduction number $\mathcal{R}_0$ and the number of initially colonized or contaminated individuals were varied.

5.5.1 Heatmap analysis

Figure 5.4 presents extinction probabilities as heatmaps across the parameter space. Panels (5.4a) and (5.4b) show extinction percentages when the outbreak is seeded by colonized patients ($P_C(0)$) or contaminated healthcare workers ($H_C(0)$), respectively.

The colour scale is mapped so that green corresponds to higher extinction probability (outbreak dies out) and red corresponds to lower extinction probability (outbreak persists).

The two seeding pathways display distinct extinction patterns. When outbreaks are initiated by colonized patients (Figure 5.4a), extinction probability is high (green) across much of the low-transmissibility parameter space and for small numbers of initial colonized patients. However, as $\mathcal{R}_0$ and $P_C(0)$ increase the heatmap shifts toward orange and red, indicating substantially reduced extinction probabilities and an increased likelihood of sustained transmission. Thus, large patient-seeding events and/or higher transmissibility markedly reduce the chance of stochastic die-out.

By contrast, outbreaks seeded by contaminated HCWs (Figure 5.4b) generally exhibit larger green regions, indicating that HCW introductions are more likely to die out spontaneously across much of the explored parameter space. Only when both $\mathcal{R}_0$ is high and many HCWs are initially contaminated do extinction probabilities fall (more orange/red), showing that widespread HCW contamination in high-transmission settings can still produce persistent outbreaks.

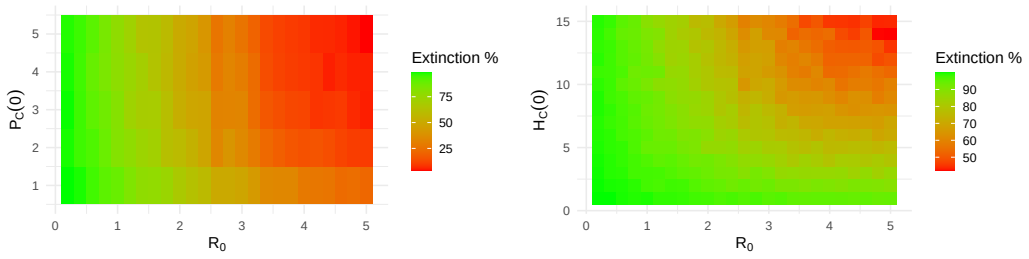

(a) Patients (b) HCWs

Figure 5.4: Heatmap of extinction probability across part of parameter space, averaged over 1000 stochastic simulations per parameter combination. The colour gradient indicates the likelihood of infection die-out, highlighting regions of parameter space where extinction is more or less probable.

5.5.2 Line analysis

To complement the heatmap analysis (Figure 5.4), we examined extinction probabilities as a function of $\mathcal{R}_0$, stratified by different levels of initial colonization/contamination (Figure 5.5). Specifically, we considered $P_C(0) \in (0, 5]$ for patient seeding and $H_C(0) \in (0, 15]$ for HCW seeding, enabling us to capture how the magnitude of the initial introduction influences extinction dynamics.

For patient seeding (Figure 5.5a), extinction probability decreases sharply with increasing $\mathcal{R}_0$, particularly when more colonized patients are present at the start of the outbreak. When $P_C(0)$ is small, extinction remains relatively likely at low $\mathcal{R}_0$ values; however, as $P_C(0)$ increases, extinction probabilities drop quickly, highlighting the importance of initial patient colonization size.

In contrast, for HCW seeding (Figure 5.5b), extinction probabilities generally remain higher across much of the $\mathcal{R}_0$ range, and the decline with increasing $\mathcal{R}_0$ is more gradual. The wider shaded uncertainty bands indicate greater stochastic variability, reflecting the more direct transmission pathway via HCWs. Notably, only when both $\mathcal{R}_0$ is large and $H_C(0)$ is high do extinction probabilities fall substantially, suggesting that widespread HCW contamination is necessary to sustain outbreaks.

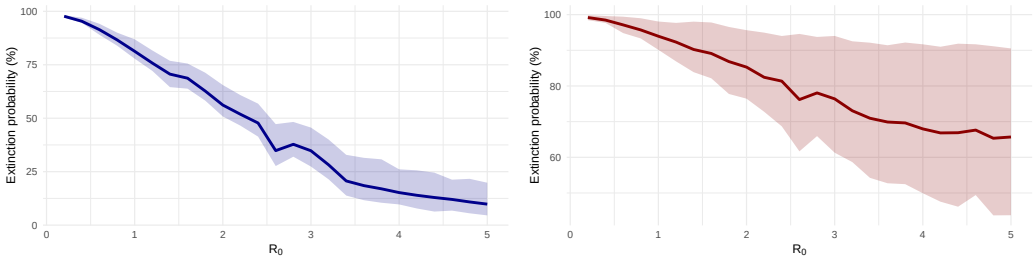

(a) Patients (b) HCWs

Figure 5.5: Extinction probability as a function of $\mathcal{R}_0$, averaged over 1000 stochastic simulations. Solid lines indicate mean extinction probability; shaded regions denote 95% confidence intervals.

Together, the heatmap and line analyses highlight the contrasting extinction dynamics between patient- and HCW-seeded outbreaks. Colonized patients represent

the more potent and persistent seeding source - especially when the number of colonized patients or $\mathcal{R}_0$ is large - whereas HCW introductions are comparatively more likely to fade out unless contamination is widespread. This underscores the importance of admission screening and rapid management of colonized patients, alongside robust infection-control practices for HCWs.

5.6 Infection origin and temporal dynamics

While sensitivity analysis (Section 5.4) shows that environmental parameters such as transmission via surfaces, contamination, and decontamination rates, are the most influential in shaping $\mathcal{R}_0$, further analysis (Section 5.5) demonstrates that the origin of infection plays a critical role in determining outbreak persistence and transmission dynamics.

Specifically, extinction analysis (Section 5.5) showed that when the outbreak originates from the colonized patient, the extinction probabilities drop below 40% (Figure 5.4a). In contrast, introductions from the colonized healthcare worker result in extinction probabilities rising above 40% (Figure 5.4b).

To dig further into these results with a high basic reproduction number ($\mathcal{R}_0 = 3$), Figures 5.6 and 5.7 show the average daily number of patient admissions, discharges, and healthcare worker shift transitions over 1000 stochastic simulations for each initial infection scenario. When the index case is a colonized patient (Figure 5.6), subsequent movement of colonized (P_C) and infectious patients (I_D, I_U) and colonized healthcare workers (H_C) is clearly observed over time. This sustained transmission chain corresponds with the lower extinction probability observed in this scenario.

In contrast, Figures 5.7 representing introductions from a colonized healthcare worker show far fewer subsequent movements of colonized or infectious patients or healthcare workers. Despite ongoing patient admissions and healthcare worker shift

activity, the infection fails to propagate, supporting the high extinction rates observed in these scenarios.

This comparative analysis highlights a critical insight: although environmental transmission parameters heavily influence the reproduction number, the stochastic trajectory of an outbreak is deeply conditioned by the origin of the initial infection. Early propagation becomes far more likely if the index case is a colonized patient, emphasizing the importance of early detection and containment at the patient level in preventing nosocomial outbreaks.

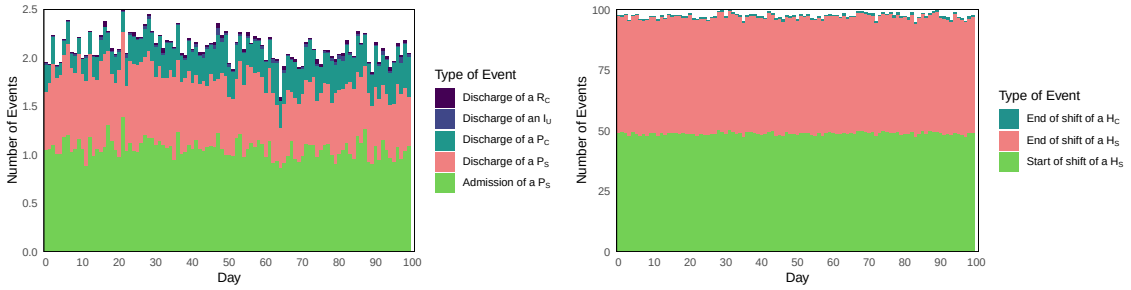

(a) Patients (b) HCWs

Figure 5.6: Average daily number of patient and HCW movements over 1000 simulations when the outbreak originates from a colonized patient. Sustained movements of colonized and infectious individuals correspond with lower extinction probabilities.

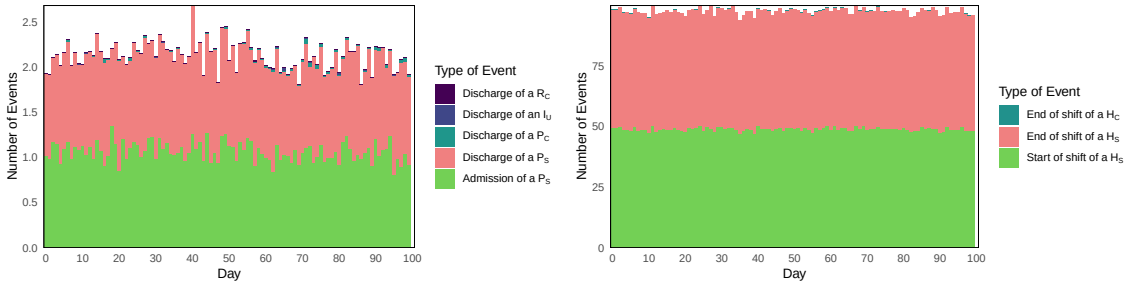

(a) Patients (b) HCWs

Figure 5.7: Average daily number of patient and HCW movements over 1000 simulations when the outbreak originates from a colonized HCW. Few colonized or infectious individuals appear, consistent with higher extinction probabilities.

5.7 Environmental transmission in established outbreaks

To further explore the role of environmental transmission once an outbreak escapes initial extinction, we analyzed secondary infection events during patient-origin scenarios. Figure 5.8 shows the average daily number of infections over 1000 simulations in which either the environment (E_C) or a colonized healthcare worker (H_C) transmitted the pathogen to susceptible patients (P_S) over a 100-day period. The results show that after a successful establishment, the environment becomes the primary conduit for sustaining transmission, with $E_C \rightarrow P_S$ events consistently outnumbering $H_C \rightarrow P_S$ transmissions.

This observation reinforces the insights from sensitivity analysis: while the origin determines whether the pathogen gains a foothold, the environment dominates as the primary transmission pathway once the outbreak is established. This underscores the critical need for rigorous environmental cleaning and contamination control strategies—particularly in scenarios where patient-origin introductions are not contained early.

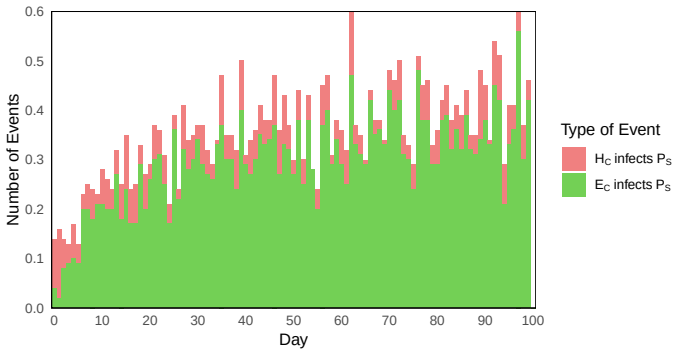

Figure 5.8: Average daily number of infection events over 1000 simulations under a patient-origin scenario, showing transmission from the environment (E_C) or colonized healthcare workers (H_C) to susceptible patients (P_S). Environmental transmission dominates once the outbreak is established.

5.8 Heatmap analysis of parameter interactions on $\mathcal{R}_0$

To further explore how combinations of epidemiologically important parameters influence the basic reproduction number $\mathcal{R}_0$, we conduct a series of heatmap analyses across six biologically plausible parameter pairs (Figure 5.9). This approach identifies nonlinear interactions and dominant control levers that single-parameter sensitivity analysis may not capture. These interactions are especially relevant in scenarios where colonized patients initiate the outbreak, as multiple transmission pathways—particularly environmental and indirect routes—contribute to sustaining transmission.

The interaction between patient discharge rate d_P and patient admission rate b_P (Figure 5.9a) shows a steep and nonlinear increase in $\mathcal{R}_0$ when both colonization duration (i.e., $1/d_P$) and admission flow are high. Accumulation of colonized patients in the ICU amplifies environmental and contact-mediated transmission risks. Policies that facilitate early discharge and regulate admissions become essential for reducing transmission potential.

The heatmap combining the detection fraction ϕ and fungal residue from undetected infectious patients ψ_U (Figure 5.9b) indicates that $\mathcal{R}_0$ is more sensitive to changes in ψ_U. This reflects the outsized impact of undetected carriers on environmental contamination and supports the need to limit exposure from these individuals, possibly through blanket precautions or preemptive disinfection.

Environmental persistence and fungal residue also interact significantly. When the fungal decay rate in the environment μ_E is low (i.e., high $1/\mu_E$) and colonized patients release fungi at high rates (ψ_D; Figure 5.9c), $\mathcal{R}_0$ increases substantially. This highlights the need to isolate colonized patients and promptly remove environmental contamination.

Finally, the pairing of $1/d_P$ and ψ_C (Figure 5.9d) further shows that the longer duration of colonization, combined with the high fungal residue, markedly amplifies $\mathcal{R}_0$. Reducing both the length of colonization and fungal residue becomes critical for outbreak control.

Across all interactions, colonization duration ($1/d_P$), environmental fungal decay rate ($1/\mu_E$), and fungal pathogen release from colonized patients (ψ_C) consistently emerge as key drivers of transmission potential. While detection (ϕ) contributes, its influence is often secondary. Effective control strategies must therefore prioritize reducing patient colonization, enhancing environmental hygiene, and minimizing fungal residue, particularly in high-risk ICU settings.

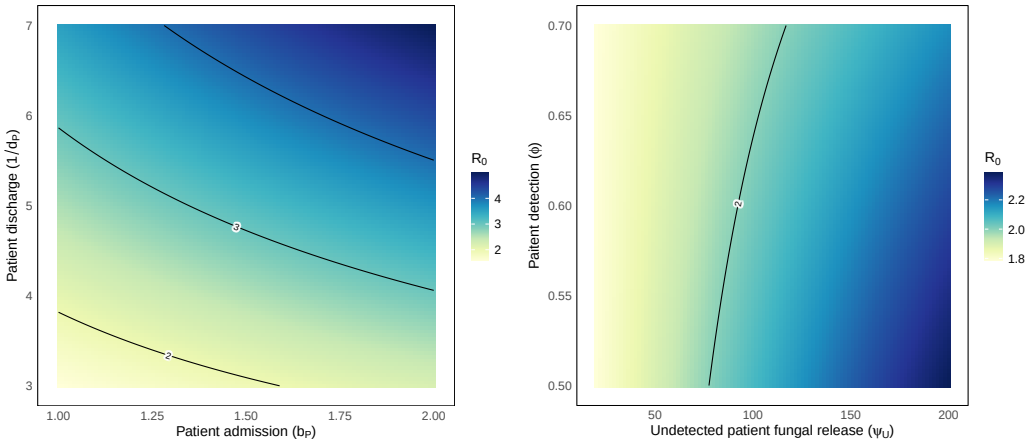

(a) b_P and d_P

(b) ψ_U and ϕ

(c) ψ_C and μ_E

(d) ψ_C and d_P

Figure 5.9: Heatmaps illustrating the combined effects of parameter pairs on the basic reproduction number $\mathcal{R}_0$ for *C. auris* transmission in an ICU setting. The pairs analyzed are: (a) patient discharge rate (d_P) vs. patient admission rate (b_P), (b) detection fraction (ϕ) vs. pathogen released by undetected infectious patients (ψ_U), (c) environmental fungal decay rate (μ_E) vs. pathogen released by colonized patients (ψ_C), (e) d_P vs. ψ_C. Color gradients represent values of $\mathcal{R}_0$, with darker regions indicating higher transmission potential. Parameter ranges correspond to those defined in Table 3.2.

6

Discussion

This study presents a modelling framework, using deterministic and stochastic approaches, to investigate the transmission dynamics of *Candida auris* in intensive care units (ICUs), a setting where colonization and environmental persistence critically shape nosocomial infection risks. Through systematic computational analysis—including sensitivity testing, extinction dynamics, parameter interaction heatmaps, and temporal dynamics—we identify the primary transmission pathways, contextualize their relative impact, and delineate actionable strategies for outbreak prevention and control.

Our parameterization strategy uses Canadian healthcare data together with biological and clinical insights from the literature, ensuring the model reflects real-world epidemiology and that the assumptions and data sources are clear and easy to follow. The global sensitivity analysis shows that environmental transmission rate (β_E), fungal release by colonized patients (ψ_C), and the duration of patient colonization ($1/d_P$) are the most influential factors governing the basic reproduction number ($\mathcal{R}_0$). These findings underscore the central role of the hospital environment as a reservoir for fungal persistence and secondary transmission.

Extinction analyses conducted via continuous-time Markov chain (CTMC) sim-

ulations further show that the origin of infection is a critical determinant of outbreak persistence. When the index case is a colonized patient, the probability of spontaneous extinction remains low—even under high-decontamination scenarios—highlighting the importance of patient-level screening and containment. In contrast, outbreaks originating from healthcare workers or contaminated surfaces tend to self-extinguish, suggesting that not all introductions pose equal threat.

Notably, the $E_C \rightarrow P_C$ pathway (mean $R_{15} = 28.16$) and $I_U \rightarrow E_C$ pathway (mean $R_{53} = 22.5$) emerge as the most significant, reinforcing the dominance of environmental contamination and undetected infectious patients in driving the epidemic. The $H_C \rightarrow P_C$ pathway (mean $R_{14} = 9.43$) indicates a secondary but notable role for healthcare workers, while other routes show minimal contribution. This matrix-based insight complements the extinction findings, emphasizing the need to target high-impact pathways early in an outbreak.

Temporal dynamics of infection trajectories reinforce this conclusion. Only patient-origin scenarios generate sustained transmission chains involving both patients and healthcare workers. Once established, the environment rapidly becomes the dominant medium of transmission, as shown by the frequency of $E_C \rightarrow P_S$ infection events surpassing those from colonized HCWs. This secondary role of the environment confirms the need for rigorous environmental cleaning protocols, especially when early containment fails.

Our heatmap analysis of biologically plausible parameter interactions builds upon these insights. We uncover several nonlinear synergies—such as between colonization duration and pathogen residue intensity, or between fungal decay and detection inefficiency—that amplify transmission risk. These interactions demonstrate that control interventions should not target parameters in isolation; instead, combined strategies are essential for curbing the reproduction number below the epidemic threshold.

Taken together, our findings recommend a tiered control strategy for high-risk ICU settings. At the entry level, aggressive screening and isolation of colonized patients are critical to prevent establishment of infection. At the system level, optimizing discharge policies, reducing colonization duration, and enhancing cleaning efficacy directly suppress environmental amplification of transmission. While healthcare worker-related parameters show limited impact on $\mathcal{R}_0$, their role in initial containment and ongoing disinfection remains valuable.

Finally, this work illustrates the strength of using deterministic and stochastic modelling in presenting complex, nonlinear, and probabilistic aspects of nosocomial pathogen spread—especially for emerging fungal threats like *C. auris*, where data are sparse and uncertainty is high. The different model approach enhances robustness, with deterministic analyses providing baseline dynamics and CTMC simulations capturing stochastic variability. Future extensions may include incorporating spatial dynamics, patient heterogeneity, and cost-effectiveness modelling of targeted interventions. Ultimately, this framework offers both a mechanistic and actionable lens for understanding ICU-based transmission of multidrug-resistant fungal pathogens.

References

[1] UK Health Security Agency. Candida auris: a review of recent literature, 2023.

[2] L.J.S Allen. An introduction to stochastic epidemic models. In *Mathematical Epidemiology*, volume 1945, pages 81–130. Springer, Berlin, Heidelberg, 2008.

[3] W.J. Anderson. *Continuous-time Markov chains: An applications-oriented approach*. Springer Science & Business Media, 2012.

[4] D. J Austin, M. J. M Bonten, R. A Weinstein, S. Slaughter, and R. M Anderson. A dynamic model for the transmission of antibiotic-resistant bacteria in hospitals. *Proceedings of the National Academy of Sciences*, 96(12):6908–6913, 1999.

[5] S. L Barnes, A. D Harris, B. L Golden, R. P Wenzel, and E. N Perencevich. Mathematical modelling of clostridium difficile transmission and control in healthcare settings: A review. *Infection Control & Hospital Epidemiology*, 31(8):755–761, 2010.

[6] F. Briano, L. Magnasco, C. Sepulcri, S. Dettori, C. Dentone, M. Mikulska, L. Ball, A. Vena, C. Robba, N. Patroniti, et al. Candida auris candidemia in critically ill, colonized patients: cumulative incidence and risk factors. *Infectious Diseases and Therapy*, 11(3):1149–1160, 2022.

[7] G.D. Brown, D.W. Denning, N.A.R. Gow, S.M. Levitz, M.G. Netea, and T.C.

White. Hidden killers: human fungal infections. *Science Translational Medicine*, 4(165):165rv13–165rv13, 2012.

[8] C. J Clancy and M. H Nguyen. Candida auris: an emerging fungal pathogen. *Journal of Clinical Microbiology*, 55(2):329–334, 2017.

[9] F. Di Ruscio, G. Guzzetta, J.V. Bjørnholt, T.M. Leegaard, A.E.F. Moen, S. Merler, and B. Freiesleben de Blasio. Quantifying the transmission dynamics of mrsa in the community and healthcare settings in a low-prevalence country. *Proceedings of the National Academy of Sciences*, 116(29):14599–14605, 2019.

[10] D. W Eyre, A. E Sheppard, H. Madder, I. Moir, R. Moroney, T. Quan, D. Griffiths, S. George, L. Butcher, M. Morgan, et al. A candida auris outbreak and its control in an intensive care setting. *New England Journal of Medicine*, 379(14):1322–1331, 2018.

[11] Centers for Disease Control and Prevention. Hand hygiene guidance, 2020. Available at: `https://www.cdc.gov/handhygiene/providers/index.html`.

[12] Canadian Institute for Health Information. Care in canadian icus — data tables, 2024.

[13] Canadian Institute for Health Information. Hospital stays in canada, 2022–2023, 2024.

[14] J.C. Kamgang and G. Sallet. Computation of threshold conditions for epidemiological models and global stability of the disease-free equilibrium (DFE). *Mathematical Biosciences*, 213(1):1–12, 2008.

[15] M. Kordalewska, Y. Zhao, S.R. Lockhart, A. Chowdhary, I. Berrio, and D.S. Perlin. Rapid and accurate molecular identification of the emerging multidrug-resistant pathogen Candida auris. *Journal of Clinical Microbiology*, 55(8):2445–2452, 2017.

[16] C. Kuhn et al. Mathematical modeling of nosocomial infections: insights into transmission dynamics and control. *Current Opinion in Infectious Diseases*, 32(4):401–407, 2019.

[17] N. H Leung and colleagues. Modeling environmental and healthcare worker-mediated transmission of candida auris in healthcare settings. *Infection Control & Hospital Epidemiology*, 44(2):234–241, 2023.

[18] S. R Lockhart. Candida auris for the clinical microbiology laboratory: not your grandfather's candida species. *Clinical Microbiology Newsletter*, 39(13):99–103, 2017.

[19] S.R. Lockhart, K.A. Etienne, S. Vallabhaneni, J. Farooqi, A. Chowdhary, N.P. Govender, A. L. Colombo, B. Calvo, C.A. Cuomo, C.A. Desjardins, et al. Editor's choice: Simultaneous emergence of multidrug-resistant Candida auris on 3 continents confirmed by whole-genome sequencing and epidemiological analyses. *Clinical Infectious Diseases: An Official Publication of the Infectious Diseases Society of America*, 64(2):134, 2017.

[20] J. Medlock, M. Kot, and A. P Galvani. Optimizing control of hospital-acquired infections: The role of modeling. *Proceedings of the National Academy of Sciences*, 106(22):8633–8638, 2009.

[21] J. D Murray. *Mathematical Biology I: An Introduction*, volume 17 of *Interdisciplinary Applied Mathematics*. Springer, New York, 3 edition, 2002.

[22] J.R. Norris. *Markov chains*. Number 2. Cambridge University Press, 1998.

[23] Public Health Agency of Canada. Candida auris: Infectious substances pathogen safety data sheet, 2023.

[24] Public Health Agency of Canada. Candida auris infection prevention and control in canadian healthcare settings, 2024.

[25] World Health Organization. Who guidelines on hand hygiene in health care: First global patient safety challenge – clean care is safer care, 2009.

[26] J. Osei Sekyere. Candida auris: A systematic review and meta-analysis of current updates on an emerging multidrug-resistant pathogen. *Microbiologyopen*, 7(4):e00578, 2018.

[27] S. Schelenz, F. Hagen, J.L. Rhodes, A. Abdolrasouli, A. Chowdhary, A. Hall, L. Ryan, J. Shackleton, R. Trimlett, J.F. Meis, et al. First hospital outbreak of the globally emerging Candida auris in a European hospital. *Antimicrobial Resistance & Infection Control*, 5(1):1–7, 2016.

[28] D. L Smith, J. Dushoff, E. N Perencevich, A. D Harris, and S. A Levin. Modelling the spread of infection in hospitals: A review. *Journal of the Royal Society Interface*, 5(16):823–841, 2008.

[29] M. Snayd, F. Dias, R.W. Ryan, D. Clout, and D.B. Banach. Misidentification of Candida auris by rapid yeast plus, a commercial, biochemical enzyme-based manual rapid identification system. *Journal of Clinical Microbiology*, 56, 2018.

[30] S. Vallabhaneni, A. Kallen, S. Tsay, N. Chow, R. Welsh, J. Kerins, S.K. Kemble, M. Pacilli, S.R. Black, E. Landon, et al. Investigation of the first seven reported cases of Candida auris, a globally emerging invasive, multidrug-resistant fungus—United States, May 2013–August 2016. *Morbidity and Mortality Weekly Report*, 65(44):1234–1237, 2016.

[31] P. van den Driessche and J. Watmough. Reproduction numbers and subthreshold endemic equilibria for compartmental models of disease transmission. *Mathematical Biosciences*, 180(1-2):29–48, 2002.

[32] X. Wang, Y. Xiao, J. Wang, and X. Lu. A mathematical model of effects of

environmental contamination and presence of volunteers on hospital infections in China. *Journal of Theoretical Biology*, 293:161–173, 2012.

[33] R. M Welsh, M. L Bentz, A. Shams, E. Adams, K. Forsberg, S. Vallabhaneni, B. R Jackson, A. P Litvintseva, and A. V Gundlapalli. Modeling the transmission and control of candida auris in healthcare settings. *Emerging Infectious Diseases*, 28(1):21–29, 2022.